Global constraints on absolute neutrino masses and their ordering

Francesco Capozzi,[1] Eleonora Di Valentino,[2,3] Eligio Lisi,[4] Antonio Marrone,[5,4]
Alessandro Melchiorri,[6,7] and Antonio Palazzo[5,4]

[1]*Department of Physics, Ohio State University, Columbus, Ohio 43210, USA*
[2]*Institut d'Astrophysique de Paris (UMR7095: CNRS & UPMC-Sorbonne Universités), F-75014 Paris, France*
[3]*Sorbonne Universités, Institut Lagrange de Paris (ILP), F-75014 Paris, France*
[4]*Istituto Nazionale di Fisica Nucleare, Sezione di Bari, Via Orabona 4, 70126 Bari, Italy*
[5]*Dipartimento Interateneo di Fisica "Michelangelo Merlin," Via Amendola 173, 70126 Bari, Italy*
[6]*Dipartimento di Fisica, Università di Roma "La Sapienza," Piazzale Aldo Moro 2, 00185 Rome, Italy*
[7]*Istituto Nazionale di Fisica Nucleare, Sezione di Roma I, Piazzale Aldo Moro 2, 00185 Rome, Italy*

(Received 16 March 2017; published 30 May 2017)

Within the standard three-neutrino framework, the absolute neutrino masses and their ordering (either normal, NO, or inverted, IO) are currently unknown. However, the combination of current data coming from oscillation experiments, neutrinoless double beta ($0\nu\beta\beta$) decay searches, and cosmological surveys, can provide interesting constraints for such unknowns in the sub-eV mass range, down to $O(10^{-1})$ eV in some cases. We discuss current limits on absolute neutrino mass observables by performing a global data analysis that includes the latest results from oscillation experiments, $0\nu\beta\beta$ decay bounds from the KamLAND-Zen experiment, and constraints from representative combinations of Planck measurements and other cosmological data sets. In general, NO appears to be somewhat favored with respect to IO at the level of $\sim 2\sigma$, mainly by neutrino oscillation data (especially atmospheric), corroborated by cosmological data in some cases. Detailed constraints are obtained via the χ^2 method, by expanding the parameter space either around separate minima in NO and IO or around the absolute minimum in any ordering. Implications for upcoming oscillation and nonoscillation neutrino experiments, including β-decay searches, are also discussed.

DOI: 10.1103/PhysRevD.95.096014

I. INTRODUCTION

Neutrino oscillation experiments have established that the three known flavor states ν_α ($\alpha = e,\ \mu,\ \tau$) are linear combinations of three massive states ν_i ($i = 1,\ 2,\ 3$) with different masses m_i, via a mixing matrix $U_{\alpha i}$ characterized by three nonzero angles θ_{ij} [1]. Flavor oscillation frequencies in vacuum are governed by the squared mass differences Δm^2_{ij} that can be expressed in terms of two independent parameters, conventionally chosen herein as [2]

$$\delta m^2 = m_2^2 - m_1^2 > 0, \tag{1}$$

$$\Delta m^2 = m_3^2 - (m_2^2 + m_1^2)/2, \tag{2}$$

where Δm^2 can be either positive or negative according to the so-called normal ordering (NO) or inverted ordering (IO) for the neutrino mass spectrum, respectively. Probing the mass ordering is an important goal of future experimental ν oscillation searches (see, e.g., [3,4]), with relevant implications on theoretical models for neutrino mass and mixing (see, e.g., [5–7]).

At present, the four parameters δm^2, $|\Delta m^2|$, $\sin^2\theta_{12}$, and $\sin^2\theta_{13}$ have been measured at the few percent level, while $\sin^2\theta_{23}$ (still affected by an octant ambiguity [8]) is less accurately known, at the level of $\sim 10\%$ [1]. Interestingly, the combination of various oscillation data starts to show some sensitivity to the remaining unknowns, namely, the sign of Δm^2 and a possible CP-violating phase δ, mainly through subleading $\nu_\mu \to \nu_e$ oscillation effects in atmospheric and accelerator neutrino experiments, constrained by reactor data [9,10]; see also [11,12] for independent analyses of oscillation data and for discussions of the associated parameters.

The absolute ν masses are also unknown. Lower bounds are set by oscillation data by zeroing the lightest m_i,

$$(m_1, m_2, m_3) \geq \begin{cases} (0, \sqrt{\delta m^2}, \sqrt{|\Delta m^2| + \delta m^2/2}) & \text{(NO)}, \\ (\sqrt{|\Delta m^2| - \delta m^2/2}, \sqrt{|\Delta m^2| + \delta m^2/2}, 0) & \text{(IO)}, \end{cases} \tag{3}$$

while upper bounds (and prospective measurements) can only be set by nonoscillation neutrino experiments. In particular, three main observables can probe the absolute mass spectrum: (i) the effective neutrino mass m_β in β decay; (ii) the effective mass $m_{\beta\beta}$ in neutrinoless double beta ($0\nu\beta\beta$) decay, if neutrinos are Majorana fermions; and

(iii) the total neutrino mass Σ in cosmology; see, e.g., the reviews in [13–16].

These observables probe the neutrino mass spectrum in different and complementary ways [1,2]. The β decay spectrum is sensitive to an (unresolved) combination of squared masses, weighted by the corresponding ν_e admixture,

$$m_\beta = \sqrt{\sum_i |U_{ei}|^2 m_i^2}, \tag{4}$$

while the $0\nu\beta\beta$ decay rate depends linearly on the m_i's via unknown Majorana phases ϕ_i (with $\phi_1 = 0$ by convention),

$$m_{\beta\beta} = \left| \sum_i \left| U_{ei} \right|^2 m_i e^{\imath\phi_i} \right|, \tag{5}$$

and cosmology essentially probes the (flavor-blind) total gravitational charge,

$$\Sigma = m_1 + m_2 + m_3. \tag{6}$$

Currently, the most constraining bounds on $m_{\beta\beta}$ can be as low as $O(0.1)$ eV in the KamLAND-Zen experiment at $\sim 2\sigma$, by assuming favorable nuclear matrix elements [17]. Upper bounds on Σ, dominated by Planck data, can also reach the level of $O(0.1)$ eV, by assuming the standard cosmological model [18,19]. Such limits are getting close to the mass scale $\sqrt{|\Delta m^2|} \simeq 0.05$ eV appearing in Eq. (3) where some sensitivity of cosmological data to mass ordering may be emerging [15]. Bounds on m_β, although free from specific assumptions, are an order of magnitude weaker at present [1,14]. In all cases, significant improvements—and possibly a positive detection—may be expected in the next decade of experimental searches [20]. In this context, we find it worthwhile to perform and discuss an updated global analysis of both oscillation and nonoscillation data, building upon previous work on the subject [21–23].

In particular, we shall highlight some interesting features emerging from the analysis of recent data (circa 2017), namely: (i) an increasing sensitivity to the mass ordering, with NO generally favored over IO at the $\sim 2\sigma$ level; (ii) differences in the allowed parameter space arising when such NO-IO offset is (not) taken into account; (iii) synergies between bounds on $m_{\beta\beta}$ and Σ of comparable strength, especially for best-fit values of Σ far from the extrema in Eq. (3). The discussion of such features also allows one to gauge the impact of prospective (non)oscillation bounds—or signals—on our knowledge of the absolute neutrino mass spectrum and its associated observables.

Our work is structured as follows. In Secs. II A, II B, and II C, we report and discuss detailed constraints coming from separate analyses of oscillations, $m_{\beta\beta}$, and Σ, respectively. In Sec. III we perform a combined analysis in the $(m_{\beta\beta}, \Sigma)$ parameter space for representative cosmological data sets. In Sec. IV we discuss the implications of such results for upcoming or prospective experiments sensitive to m_β. A brief summary is presented in Sec. V.

II. DATA SETS, STATISTICAL ANALYSIS, AND PARAMETER BOUNDS

In this paper, all the bounds on the mass-mixing parameters coming from various (separate or combined) data sets are expressed in terms of $\Delta\chi^2$ differences with respect to a minimum χ^2 value. In particular, the differences

$$\Delta\chi^2 = n^2 \tag{7}$$

are used to derive $n\sigma$ allowed regions. Projections of such regions onto a single parameter provide the $\pm n\sigma$ range(s) for that parameter [24]. In all figures, it is understood that the undisplayed parameters are projected away (i.e., marginalized). Following the general statistical arguments in [25], we use the $\Delta\chi^2$ metric also to assess the relative likelihood of the two mass-ordering hypotheses,

$$\Delta\chi^2_{\mathrm{IO-NO}} = \chi^2_{\mathrm{min,IO}} - \chi^2_{\mathrm{min,NO}}. \tag{8}$$

From a historical viewpoint, an interesting parallel to the metric in Eq. (8) can be found in the development of solar neutrino data analyses. In the early literature, different and seemingly disconnected oscillation solutions to the solar neutrino problem (e.g., the so-called matter and vacuum solutions) were often analyzed via separate fits around the corresponding χ^2 minima in the $(\delta m^2, \sin^2 2\theta_{12})$ parameters (see, e.g., [26,27]), and possibly compared to each other by tests of hypotheses. However, when diverse solutions were explicitly connected in the $(\delta m^2, \sin^2\theta_{12})$ or $(\delta m^2, \tan^2\theta_{12})$ variables [28–31], it became customary to expand the fit around the absolute χ^2 minimum and to compare different solutions by a $\Delta\chi^2$ parameter test [1,32,33]—until a single one was eventually found by solar and long-baseline reactor experiments [34].

The comparison of the two mass orderings seem to follow an analogous path. On the one hand, one may take NO and IO as two alternative options, involving separate fits and tests of hypotheses. On the other hand, one may try to connect them through a continuous variable, involving a parameter estimation test. Such a variable could be either physical (e.g., Δm^2, ranging from negative to positive real values) or unphysical (e.g., a fudge parameter $p \in [0, 1]$ linking any two competing hypotheses [35]). Explicit parametric connections have been worked out for medium-baseline reactor neutrino oscillations, in terms of the mixing variable $\sin^2\theta_{12}$ (swapping octants between NO and IO for $\Delta m^2 > 0$ in vacuum [36]) and of an empirical variable α (ranging in $[-1, +1]$ from IO to NO [37]). The above considerations further support our

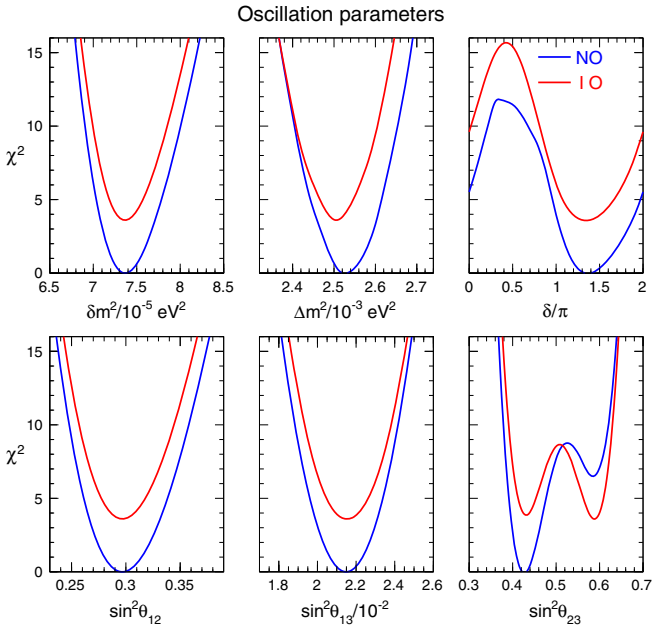

FIG. 1. Global 3ν oscillation analysis. Projections of the χ^2 function onto the parameters δm^2, $|\Delta m^2|$, $\sin^2\theta_{ij}$, and δ, for NO (blue curves) and IO (red curves). In each panel, all the undisplayed parameters are marginalized, and the offset $\Delta\chi^2_{\mathrm{IO-NO}} = 3.6$ is included.

adoption of Eq. (8) as a reasonable metric for the IO-NO discrimination [25], akin to a one-parameter estimation test. For a discussion of further statistical issues and possible alternative approaches, see also [3,4,38–40] and references therein.

With the present data, the current statistical sensitivity associated with $\Delta\chi^2_{\mathrm{IO-NO}}$ tests appears to be limited to $\sim 2\sigma$ (see Sec. III). Therefore, we shall conservatively report $\Delta\chi^2$ bounds on mass-mixing parameters both by *separately* minimizing the χ^2 in NO and IO (discarding the relative $\Delta\chi^2_{\mathrm{IO-NO}}$ difference) and by further minimizing the χ^2 over *any* ordering (including the $\Delta\chi^2_{\mathrm{IO-NO}}$ information), with a discussion of the relative differences in the results. Such a format has been adopted in presenting the oscillation parameter ranges in [11,41] and is extended herein to nonoscillation parameters.

A. Neutrino oscillations

An analysis of neutrino oscillation data has been previously presented in [9], to which we refer the reader for a discussion of the adopted methodology and earlier literature. A partial update of [9], including novel accelerator data shown in mid-2016, was reported in [10]. The more complete update presented herein (circa 2017) includes, with respect to [9]: (i) the latest results from the long-baseline accelerator experiments T2K [42] and NOvA [43,44]; (ii) the latest far/near spectral ratio from the reactor neutrino experiment Daya Bay [45]; (iii) the most recent atmospheric neutrino data from the Super-Kamiokande (SK) phase IV [46,47]. The results of our oscillation data analysis are reported graphically in Fig. 1 and numerically in Table I.

Figure 1 shows the χ^2 curves in terms of the six oscillation parameters $(\delta m^2, \Delta m^2, \sin^2\theta_{12}, \sin^2\theta_{13}, \sin^2\theta_{23}, \delta)$, for both NO (blue curves) and IO (red curves). We find an overall preference for NO, quantified by the χ^2 difference

$$\Delta\chi^2_{\mathrm{IO-NO}} = 3.6 (\text{all oscill. data}) \tag{9}$$

TABLE I. Results of the global 3ν oscillation analysis, in terms of best-fit values for the mass-mixing parameters and associated $n\sigma$ ranges ($n = 1, 2, 3$), defined by $\chi^2 - \chi^2_{\mathrm{min}} = n^2$ with respect to the separate minima in each mass ordering (NO, IO) and to the absolute minimum in any ordering. (Note that the fit to the δm^2 and $\sin^2\theta_{12}$ parameters is basically insensitive to the mass ordering.) We recall that Δm^2 is defined herein as $m^2_3 - (m^2_1 + m^2_2)/2$ and that δ is taken in the (cyclic) interval $\delta/\pi \in [0, 2]$.

Parameter	Ordering	Best fit	1σ range	2σ range	3σ range
$\delta m^2/10^{-5}$ eV^2	NO, IO, any	7.37	7.21–7.54	7.07–7.73	6.93–7.96
$\sin^2\theta_{12}/10^{-1}$	NO, IO, any	2.97	2.81–3.14	2.65–3.34	2.50–3.54
$\lvert\Delta m^2\rvert/10^{-3}$ eV^2	NO	2.525	2.495–2.567	2.454–2.606	2.411–2.646
	IO	2.505	2.473–2.539	2.430–2.582	2.390–2.624
	Any	2.525	2.495–2.567	2.454–2.606	2.411–2.646
$\sin^2\theta_{13}/10^{-2}$	NO	2.15	2.08–2.22	1.99–2.31	1.90–2.40
	IO	2.16	2.07–2.24	1.98–2.33	1.90–2.42
	Any	2.15	2.08–2.22	1.99–2.31	1.90–2.40
$\sin^2\theta_{23}/10^{-1}$	NO	4.25	4.10–4.46	3.95–4.70	3.81–6.15
	IO	5.89	4.17–4.48 ⊕ 5.67–6.05	3.99-4.83 ⊕ 5.33–6.21	3.84–6.36
	Any	4.25	4.10–4.46	3.95–4.70 ⊕ 5.75–6.00	3.81–6.26
δ/π	NO	1.38	1.18–1.61	1.00–1.90	0–0.17 ⊕ 0.76–2
	IO	1.31	1.12–1.62	0.92–1.88	0–0.15 ⊕ 0.69–2
	Any	1.38	1.18–1.61	1.00–1.90	0–0.17 ⊕ 0.76–2

that is explicitly shown as an offset of the IO curves. The offset is of some relevance in the analysis of absolute mass observables, as shown later.

Table I reports best-fit values and parameter ranges for separate χ^2 minimization in each separate ordering (NO and IO) and in any ordering; the latter case takes into account the above $\Delta\chi^2_{\text{IO-NO}}$ value. The known parameters $(\delta m^2, |\Delta m^2|, \sin^2\theta_{12}, \sin^2\theta_{13})$, which affect the absolute mass observables in Eqs. (4)–(6), are determined with a fractional 1σ accuracy (defined as $1/6$ of the $\pm 3\sigma$ range) of (2.3, 1.6, 5.8, 4.0) percent, respectively. For such parameters, it turns out that minimization in any ordering reproduces the same allowed ranges as for NO. Given the δm^2 and Δm^2 estimates in Table I, Eq. (3) becomes

$$(m_1, m_2, m_3) \gtrsim \begin{cases} (0, 0.86, 5.06) \times 10^{-2}\ \text{eV} & \text{(NO)}, \\ (4.97, 5.04, 0) \times 10^{-2}\ \text{eV} & \text{(IO)}. \end{cases} \quad (10)$$

The parameter $\sin^2\theta_{23}$ is less well known, at the level of 9.6%. At 3σ, its octant degeneracy is unresolved, and maximal mixing is also allowed. At lower significance, maximal mixing is disfavored in both NO and IO, and the first octant is preferred in NO. The $n\sigma$ ranges for θ_{23} for any ordering are larger than for NO (Table I), as a result of joining the NO and IO intervals determined by the curves in the right-lower panel of Fig. 1 at $\chi^2 = n^2$. Concerning the possible CP-violating phase δ, our analysis strengthens the trend in favor of $\delta \sim 3\pi/2$ [9,11,42] and disfavors ranges close $\delta \sim \pi/2$ at $\gtrsim 3\sigma$. In any case, the parameters θ_{23} and δ do not enter in the calculation of $(m_\beta, m_{\beta\beta}, \Sigma)$.

A few remarks are in order about the IO-NO offset in Eq. (9). This value is in the ballpark of the official SK fit results quoted in [46,47], namely: $\Delta\chi^2_{\text{IO-NO}} = 4.3$ (for SK data at fixed θ_{13}) and $\Delta\chi^2_{\text{IO-NO}} = 5.2$ (for SK + T2K data at fixed θ_{13}). By excluding SK atmospheric data in our fit, we find $\Delta\chi^2_{\text{IO–NO}} = 1.1$, in qualitative accord with the official T2K data analysis constrained by reactor data [42].

Concerning SK atmospheric data, it has been emphasized [9,11,12] that the complete set of bins and systematics [46,47] can only be handled within the collaboration, especially when $\nu/\bar{\nu}$ or multiring event features are involved. Nevertheless, we think it useful to continue updating our analysis of reproducible SK samples, namely, sub-/multi-GeV single-ring (e-like and μ-like) and stopping/throughgoing (μ-like) distributions. These samples encode interesting (although entangled and smeared) pieces of information about subleading effects driven by known and unknown oscillation parameters (see, e.g., [2]); in particular, they contributed to early hints of nonzero θ_{13} [48]. At present, we trace the atmospheric hint of NO to e-like events, especially multi-GeV, in qualitative agreement with [49].[1]

[1]Note, however, that weaker results for the IO-NO difference ($\lesssim 1\sigma$), with or without atmospheric data, have been found in [11].

Summarizing, the SK(+T2K) official results in [42,46,47] and ours in Eq. (9) suggest, at face value, that global 3ν oscillation analyses may have reached an overall $\sim 2\sigma$ sensitivity to the mass ordering, with a preference for NO driven by atmospheric data and corroborated by accelerator data, together with reactor constraints. This intriguing indication, although still tentative, is generally supported by cosmological data (see Sec. II C) and thus warrants a dedicated discussion in the context of absolute ν mass observables (see Sec. III).

B. Neutrinoless double beta decay

If the three known neutrinos are Majorana fermions, the rare process of $0\nu\beta\beta$ decay is expected to occur with half-life T given by

$$T^{-1} = G|M|^2 m_{\beta\beta}^2, \quad (11)$$

where $m_{\beta\beta}$ is given in Eq. (5), G is the (calculable) phase space, and M is the nuclear matrix element (NME) for a candidate nucleus [15,50–52].

A worldwide search is underway to find possible $0\nu\beta\beta$ decay signatures in a variety of nuclei, and lower limits on the corresponding half-lives have been placed [53–55]. Transforming lower bounds on T into upper bounds on $m_{\beta\beta}$ requires theoretical input on the NME and their uncertainties [15,50–52,56–58]. The strongest $m_{\beta\beta}$ limit to date is provided by the KamLAND-Zen experiment with ^{136}Xe, which finds $T > 1.07 \times 10^{26}$ yr (90% C.L.), and derives the range $m_{\beta\beta} \gtrsim 0.061$–$0.165$ eV (90% C.L.) by bracketing recent NME calculations [17]. For the sake of simplicity, we include only the (dominant) KamLAND-Zen constraints herein.

In order to derive bounds at any given C.L. in our analysis, we build a general $\chi^2(m_{\beta\beta})$ function by using the following: (i) the experimental $\chi^2(T)$ curve presented by the KamLAND-Zen Collaboration in [59] [with $T = T(m_{\beta\beta}, |M|)$ from Eq. (11)]; and (ii) our construction of the $\chi^2(|M|)$ function, based on the conservative theoretical uncertainties estimated in [60]. The objective function is obtained as

$$\chi^2(m_{\beta\beta}) = \min_{|M|}[\chi^2(T(m_{\beta\beta}, |M|)) + \chi^2(|M|)] \quad (12)$$

and is shown in Fig. 2. These results do not depend on the mass ordering and, in particular, $\Delta\chi^2_{\text{IO-NO}} = 0$.

From Fig. 2 we get $m_{\beta\beta} < 0.15$ eV at 90% C.L., close to the most conservative limit quoted at the same C.L. in [17] (0.165 eV). From Fig. 2 we also derive

$$m_{\beta\beta} < 0.18\ \text{eV at } 2\sigma (< 0.27\ \text{eV at } 3\sigma). \quad (13)$$

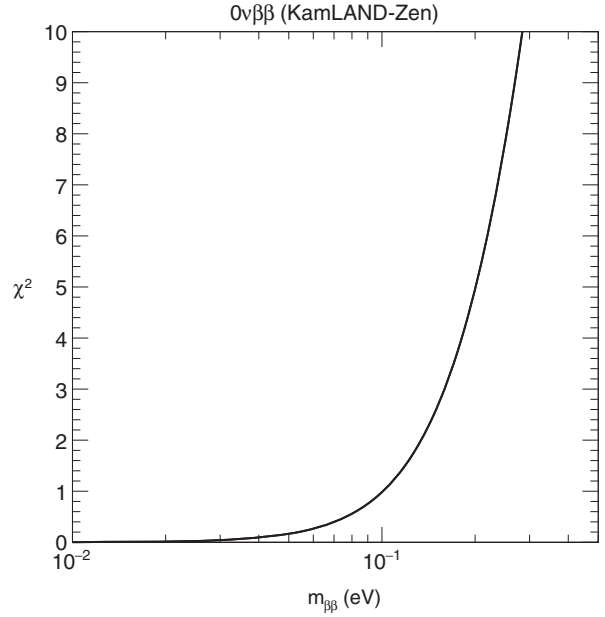

FIG. 2. Constraints from $0\nu\beta\beta$ decay, in terms of the function $\chi^2(m_{\beta\beta})$ derived from KamLAND-Zen data [17,59] and from an estimate of the ^{136}Xe nuclear matrix elements and its uncertainties based on [60]. The same constraints apply to both NO and IO. See the text for details.

For completeness, our assessment of the $\chi^2(m_{\beta\beta})$ function is detailed below.

According to [60], Eq. (11) is linearized via logarithms as $\tau = \gamma - 2\eta - 2\mu$, where $\gamma = -\log_{10}(G/\mathrm{y}^{-1}\ \mathrm{eV}^{-2})$, $\tau = \log_{10}(T/y)$, $\eta = \log_{10}(|M|)$, and $\mu = \log_{10}(m_{\beta\beta})$. The NME η and its uncertainties with respect to a central value $\bar{\eta}$ are parametrized as $\eta = \bar{\eta} + \alpha(g_A - 1) + s\beta \pm \sigma$, where g_A is the effective axial coupling (typically "quenched" with respect to the vacuum value $g_A^0 \simeq 1.27$ [15]), $s = \pm 1$ switches between two alternative approaches to short-range correlation effects (so-called charge-dependent Bonn (CD-Bonn) and Argonne potentials), while σ is a residual (nonparametric) uncertainty [60]. Numerical values for ^{136}Xe are $\gamma = 24.865$, $\bar{\eta} = 0.267$, $\alpha = 0.458$, $\beta = 0.021$, $\sigma = 0.032$.

Concerning the total 1σ uncertainty σ_η affecting η, we assume $g_A = 1 \pm 0.15$ as a reasonable 1σ estimate for the axial coupling. The central value corresponds to default quenching ($g_A = 1$) [15], and the 2σ range $g_A \in [0.7, 1.3]$ spans typical effective values adopted in the NME literature up to g_A^0 [52], while the 3σ range goes down to $g_A = 0.55$, close to the very low estimates $g_A \simeq 1.27A^{-0.18} \simeq 0.52$ considered in [15,61] (for $A = 136$). Concerning alternative short-range correlation approaches, we conservatively assume that the associated uncertainty ($s\beta = \pm\beta$) corresponds statistically to $\pm 1\sigma$. The total error σ_η is then evaluated by summing in quadrature the three independent components, namely, $\alpha \cdot 0.15 = 0.069$, $\beta = 0.021$, and $\sigma = 0.032$, leading to $\eta = \bar{\eta} \pm \sigma_\eta = 0.267 \pm 0.079$ (1σ). Finally, we minimize over η according to Eq. (12), where the second term on the right-hand side is given by $\chi^2_\eta = [(\eta - \bar{\eta})/\sigma_\eta]^2$. Our estimate $\eta = 0.267 \pm 0.079$ implies a $\pm 3\sigma$ range $|M| \simeq 1.1$–3.2, to be compared with the total range $|M| \simeq 1.6$–4.3 adopted in [17]. The overall shift is mainly related to a different choice for the default axial coupling ($g_A = 1.27$ in [17] versus $g_A = 1$ herein). In any case, both ranges correspond to a conservative factor of ~ 3 uncertainty of $|M|$.

The above results refer to a single (dominant) experimental datum for the ^{136}Xe nucleus. When comparable bounds on $m_{\beta\beta}$ will be obtained in other experiments and nuclei, the combination of various $0\nu\beta\beta$ data should take into account the theoretical NME covariances among different nuclei [62].

C. Cosmology

Neutrinos are the only known particles in the standard model of particle physics that can change behavior, from the relativistic to the nonrelativistic regime, in an epoch after CMB recombination. This change leaves a characteristic imprint on several cosmological observables (see, e.g., [16,63–67]), letting cosmology to strongly bound the neutrino mass scale, indeed providing the current strongest (albeit model dependent) bounds on Σ. Bounds on Σ from recent cosmological data have been presented in several papers (see, for example, [68–73] and references therein) while forecasts for near (and far) future cosmological data sets have been obtained in [74–79].

Clearly, current cosmological constraints on neutrino masses depend on the combination of data sets considered and on the theoretical framework assumed (see, for example, [80–85]). It is therefore important to be extremely clear in the description of the assumptions we make. In our analysis we consider six different combinations of the following data sets:

(i) The full range of the Planck 2015 temperature anisotropy angular power spectrum, both at low multipole ℓ ($2 \le \ell \le 29$) and high ℓ ($30 \le \ell \le 2508$), provided by the Planck Collaboration [86]. We define this data set as Planck TT.

(ii) The full multipole range of the Planck 2015 temperature anisotropy angular power spectrum, and high multipoles E polarization and cross TE temperature polarization anisotropy angular power spectra ($30 \le \ell \le 2508$) [86]. We define this data set as Planck TT, TE, EE.

(iii) A Gaussian prior on the reionization optical depth $\tau = 0.055 \pm 0.009$, as obtained recently from Planck high-frequency instrument (HFI) data [87]. We refer to this prior as τ_{HFI}.

(iv) The baryon acoustic oscillation measurements from 6dFGS [88], SDSS-MGS [89], BOSSLOWZ [90], and CMASS-DR11 [90] surveys as done in [19]. We label this data set as BAO.

(v) The Planck 2015 CMB lensing potential power spectrum reconstruction data [91]. We refer to this data set as "lensing."

In our analysis we always consider a flat universe, a cosmological constant, and adiabatic primordial perturbations, within the so-called ΛCDM model. However, we consider two slightly different theoretical scenarios:

(i) The "standard" $6+1$ parameters of the ΛCDM + Σ model, where the six parameters of the ΛCDM are the baryon and cold dark matter densities ω_b and ω_{cm}, the amplitude A_s and spectral index n_s of primordial density fluctuations, the Hubble constant H_0 and the reionization optical depth τ, and the seventh extra parameter Σ is also free.

(ii) An extended $6+2$ parameter scenario, considering variation also in the lensing amplitude $A_{\rm lens}$ that controls the effects of gravitational lensing in the Planck TT, TE, and EE angular spectra [92]. This parameter is expected to be $A_{\rm lens}=1$ in the standard ΛCDM model. However, the most recent Planck data analysis shows a statistically significant preference for values $A_{\rm lens}>1$ (in particular, $A_{\rm lens}=1.15^{+0.13}_{-0.12}$ at $\pm 2\sigma$) [87]. While the physical motivations behind this result are not yet clear (systematics or new physics), we consider also this parameter as free, since its correlation with Σ strongly weakens the cosmological constraints on neutrino masses. The scenario with an extra $A_{\rm lens}$ parameter is therefore expected to yield more conservative results.

The cosmological constraints are obtained using the November 2016 version of the publicly available Monte Carlo Markov chain package COSMOMC [93,94], with a convergence diagnostic based on the Gelman and Rubin statistic that implements an efficient sampling of the posterior distribution using the fast/slow parameter decorrelations [95], and that includes the support for the Planck data release 2015 likelihood code [86]. We emphasize that we implement separately the NO and IO options in the CosmoMC analysis; namely, the masses m_i entering in the definition of Σ obey the δm^2 and Δm^2 constraints in Eqs. (1) and (2). In particular, from the fit results in Table I and Eq. (10), it is

$$\Sigma = m_1 + m_2 + m_3 \gtrsim \begin{cases} 0.06 \text{ eV} & \text{(NO)}, \\ 0.10 \text{ eV} & \text{(IO)}. \end{cases} \tag{14}$$

Such an approach differs from other recent studies, where neutrino masses are assumed to be degenerate ($m_i = m \geq 0$) and the above constraints are relaxed ($\Sigma \geq 0$). In such studies, best-fit results around $\Sigma \simeq 0$ (i.e., in the unphysical region) tend to induce a somewhat artificial preference for NO over IO, just because NO allows Σ values lower than IO. For any scenario and combination of cosmological data sets, our CosmoMC fit leads, in general, to different best-fit values for Σ (in the physical region) and for the associated values of $\chi^2_{\rm min}$ in NO and IO. The value of $\Delta\chi^2_{\rm IO\text{-}NO}$ correctly quantifies the overall preference of the fitted cosmological data set for one mass ordering.

From CosmoMC one also gets the posterior probability functions $p(\Sigma)$ in NO and IO, which are transformed into $\chi^2(\Sigma)$ functions by applying [24] the standard Neyman construction [96] and Feldman-Cousins method [97]. We have also verified that, for any given cosmological data set, the resulting $\chi^2(\Sigma)$ curves for NO and IO converge for increasing Σ as they should (up to residual numerical artifacts at the level of $\delta\chi^2 \lesssim 0.1$). The χ^2 analysis of cosmological data is thus methodologically consistent with the χ^2 analysis of oscillation and $0\nu\beta\beta$ data, and a global combination of the data can be performed (see next section).

The main cosmological fit results are summarized in Table II, in terms of upper bounds (at the 2σ level) on the sum of neutrino masses Σ for NO and IO, together with the $\Delta\chi^2_{\rm NO\text{-}IO}$ offset. The results show some global trends: (a) the Σ bounds are significantly strengthened by enlarging the Planck temperature data with polarization spectra or with BAO data, while they are only moderately tightened by adding lensing data; (b) the bounds are largely weakened, up to a factor of ∼2 in some cases, by letting $A_{\rm lens}$ free.

At a finer level, slight differences emerge between the results in NO and IO in Table II, indicating a weak sensitivity of cosmological data to the mass ordering. Interestingly, normal ordering is generally preferred, except for a few cases where $\Delta\chi^2_{\rm NO\text{-}IO}$ is either negligible or slightly negative, corresponding to the extended and conservative scenario in which the $A_{\rm lens}$ parameter is varying. The overall indication in favor of NO, although still at the $\lesssim 1\sigma$ level, is consistent with the neutrino oscillation results in Eq. (9) and brings the global preference for NO at the typical level of $\Delta\chi^2 \simeq 4$ in our analysis (i.e., 2σ). Note that the overall preference for NO from cosmological data exceeds 1σ only in the case Nos. 3 and 6 of Table II that, not surprisingly, are associated with the strongest constraints on the sum of neutrino masses ($\Sigma \lesssim 0.2$ eV at 2σ) that are arising when using the BAO data, since they are directly sensitive to the free-streaming nature of the neutrinos. Moreover, the constraints of these two cases are not affected by the lowering of the optical depth, as it happens for the other combination of data sets if compared to the Planck 2015 findings [19], showing that the BAO bounds are very robust and reliable. Finally, we remark that the constraints in Table II are slightly less stringent than those reported in [87] for similar data sets, as a result of having nonzero lower limits on Σ as in Eq. (14). We have checked that, by assuming degenerate neutrino masses (with allowance for $\Sigma \to 0$) we recover almost exactly the constraints reported in [87].

Further details can be appreciated in terms of the $\chi^2(\Sigma)$ functions for NO and IO. For the sake of simplicity, we do so only for four representative cases numbered as Nos. 10,

TABLE II. Results of the global 3ν analysis of cosmological data within the standard ΛCDM + Σ and extended ΛCDM + Σ + $A_{\rm lens}$ models. The data sets refer to various combinations of the Planck power angular CMB temperature power spectrum (TT) plus polarization power spectra (TE, EE), reionization optical depth $\tau_{\rm HFI}$, lensing potential power spectrum (lensing), and BAO measurements. For each of the 12 cases we report the 2σ upper bounds on $\Sigma = m_1 + m_2 + m_3$ for NO and IO, together with the $\Delta\chi^2$ difference between the two mass orderings (with one digit after the decimal point). For any Σ, the masses m_i are taken to obey the δm^2 and Δm^2 constraints coming from oscillation data. See the text for more details.

No.	Model	Cosmological data set	Σ/eV (2σ), NO	Σ/eV (2σ), IO	$\Delta\chi^2_{\rm IO\text{-}NO}$
1	ΛCDM + Σ	Planck TT + $\tau_{\rm HFI}$	<0.72	<0.80	0.7
2	ΛCDM + Σ	Planck TT + $\tau_{\rm HFI}$ + lensing	<0.64	<0.63	0.2
3	ΛCDM + Σ	Planck TT + $\tau_{\rm HFI}$ + BAO	<0.21	<0.23	1.2
4	ΛCDM + Σ	Planck TT, TE, EE + $\tau_{\rm HFI}$	<0.44	<0.48	0.6
5	ΛCDM + Σ	Planck TT, TE, EE + $\tau_{\rm HFI}$ + lensing	<0.45	<0.47	0.3
6	ΛCDM + Σ	Planck TT, TE, EE + $\tau_{\rm HFI}$ + BAO	<0.18	<0.20	1.6
7	ΛCDM + Σ + $A_{\rm lens}$	Planck TT + $\tau_{\rm HFI}$	<1.08	<1.08	−0.1
8	ΛCDM + Σ + $A_{\rm lens}$	Planck TT + $\tau_{\rm HFI}$ + lensing	<0.91	<0.93	0.0
9	ΛCDM + Σ + $A_{\rm lens}$	Planck TT + $\tau_{\rm HFI}$ + BAO	<0.45	<0.46	0.2
10	ΛCDM + Σ + $A_{\rm lens}$	Planck TT, TE, EE + $\tau_{\rm HFI}$	<1.04	<1.03	0.0
11	ΛCDM + Σ + $A_{\rm lens}$	Planck TT, TE, EE + $\tau_{\rm HFI}$ + lensing	<0.89	<0.89	0.1
12	ΛCDM + Σ + $A_{\rm lens}$	Planck TT, TE, EE + $\tau_{\rm HFI}$ + BAO	<0.31	<0.32	0.3

1, 9, and 6 in Table II, as shown in Fig. 3. These cases lead to increasingly strong upper bounds on Σ, ranging from $\lesssim$1 eV (No. 10) to $\lesssim$0.2 eV (No. 6) at 2σ. The corresponding offset $\Delta\chi^2_{\rm IO\text{-}NO}$ ranges from ∼0 to 1.6. In two cases (Nos. 1 and 6) the χ^2 minima are reached at the extrema of Σ from Eq. (14), while in the other two (Nos. 10 and 9) they are reached at higher values. In general, we find that the cases with $A_{\rm lens}$ free lead to best-fit values of Σ above the extrema in Eq. (14) (not shown). We emphasize that, in all cases, the $\chi^2(\Sigma)$ curves for NO and IO tend to converge for degenerate masses m_i (large Σ), while they bifurcate toward the extrema in Eq. (14), corresponding to strongly hierarchical masses at low Σ. The four cases in Fig. 3 are sufficiently representative of the variety of constraints set by current cosmological data in Table II and will be explicitly considered in the global analysis of oscillation and nonoscillation neutrino data in the next section.

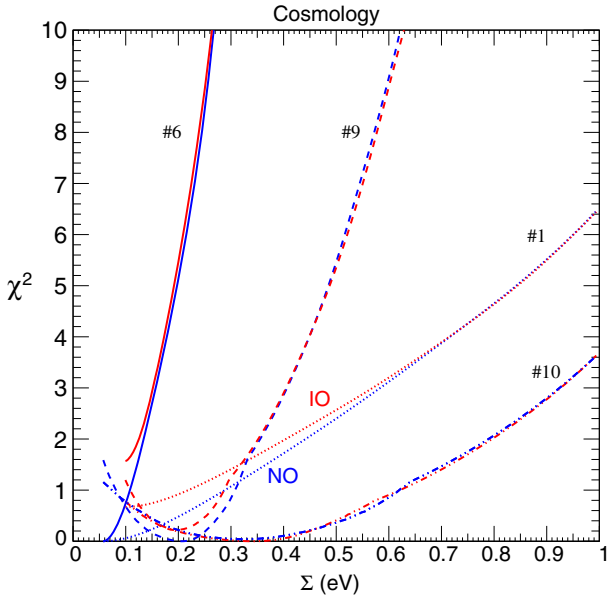

FIG. 3. Constraints on the sum of neutrino masses from cosmological data. The $\chi^2(\Sigma)$ function is shown in NO (blue curves) and IO (red curves) for four representative cases, numbered as Nos. 10, 1, 9, and 6 in Table II, and including the corresponding $\Delta\chi^2_{\rm IO\text{-}NO}$ offset. In each case, the NO and IO curves diverge as Σ approaches the extrema in Eq. (14), while they tend to converge for large Σ, as the mass ordering sensitivity vanishes.

III. COMBINED CONSTRAINTS IN THE $(\Sigma, m_{\beta\beta})$ PLANE

In this section we present increasingly strong constraints on the absolute mass observables $(\Sigma, m_{\beta\beta})$ in the (sub)eV range, obtained by combining the χ^2 from oscillation data (Fig. 1) with the χ^2 from $0\nu\beta\beta$ (Fig. 2) and then with the χ^2 from cosmological data (Fig. 3). Current β-decay constraints ($m_\beta \lesssim 2$ eV [1]) are not relevant in this context.

As discussed in Sec. II, we consider two alternative ways to obtain allowed regions: (i) the χ^2 is separately minimized on the relevant parameters in each mass ordering, either NO or IO, discarding the $\Delta\chi^2_{\rm IO\text{-}NO}$ information; and (ii) the χ^2 is further minimized over NO and IO, including the $\Delta\chi^2_{\rm IO\text{-}NO}$ information. In the former case, one should consider the NO and IO allowed regions as exclusive while, in the latter case, one should join the NO and IO allowed regions to obtain the global ones in "any ordering."

Figure 4 shows the 2σ and 3σ constraints in the $(\Sigma, m_{\beta\beta})$ plane, derived from the oscillation data discussed in Sec. II A. The left panel refers to separate fits in each mass ordering, while the right panel refers to the global fit in any ordering. The main features of the allowed bands have been discussed in previous literature (see [21,22,98–101] and references therein) and are not repeated here. We only recall

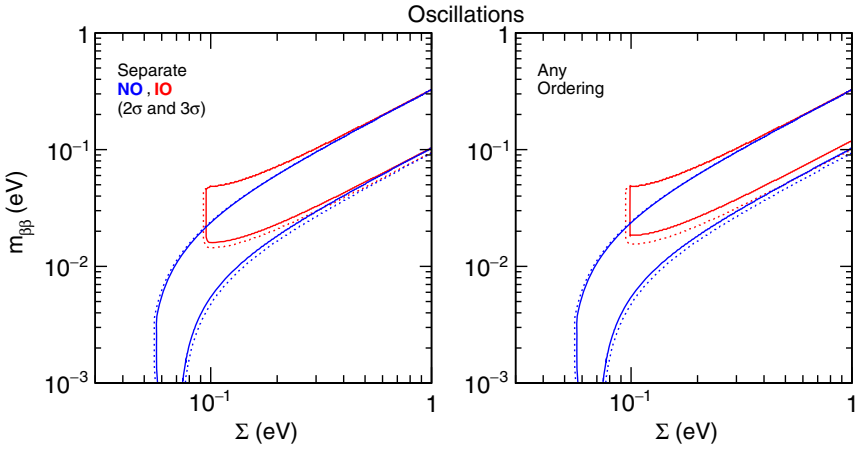

FIG. 4. Global analysis in the $(\Sigma, m_{\beta\beta})$ plane, including only oscillation data. Constraints are shown in terms of 2σ (solid curves) and 3σ (dotted curves) allowed regions for NO (blue curves) and IO (red curves). In the left panel, the χ^2 minimization is separately performed in each mass ordering, and the allowed regions should be separately considered for NO and IO. In the right panel, the χ^2 is further minimized over the mass ordering, and the allowed regions (for any ordering) are given by the union of the NO and IO ones.

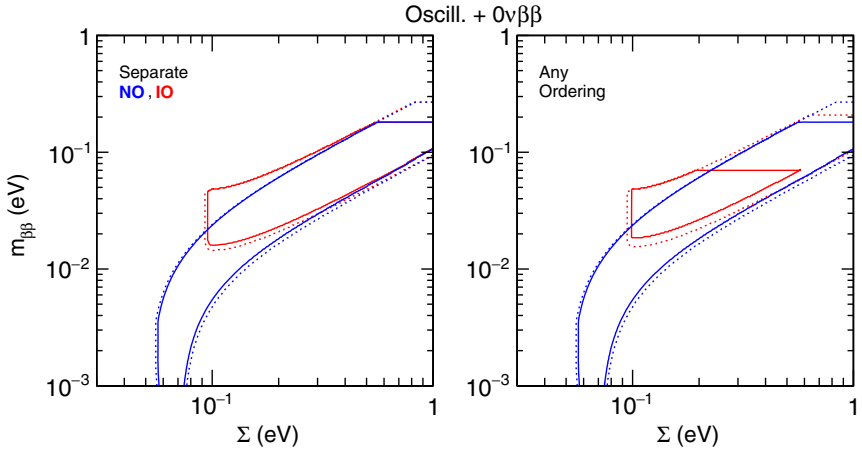

FIG. 5. As in Fig. 4, but including the $\chi^2(m_{\beta\beta})$ function from Fig. 2.

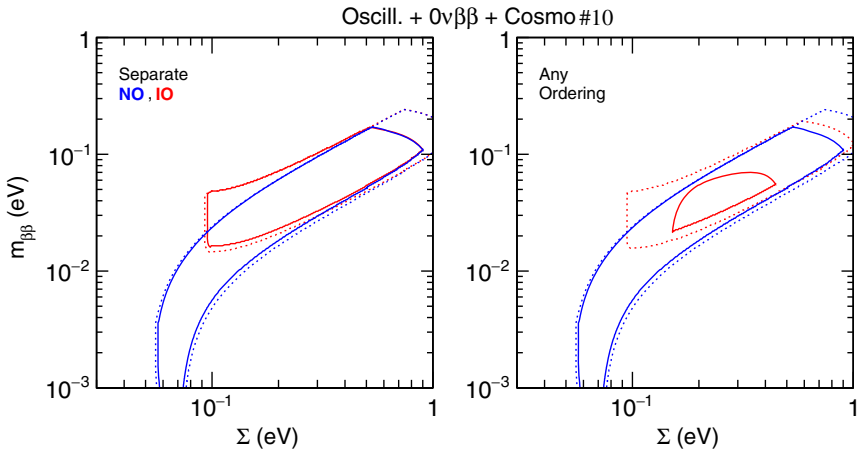

FIG. 6. As in Fig. 4, but including the $\chi^2(m_{\beta\beta})$ function from Fig. 2 and the $\chi^2(\Sigma)$ function from Fig. 3 (for case No. 10).

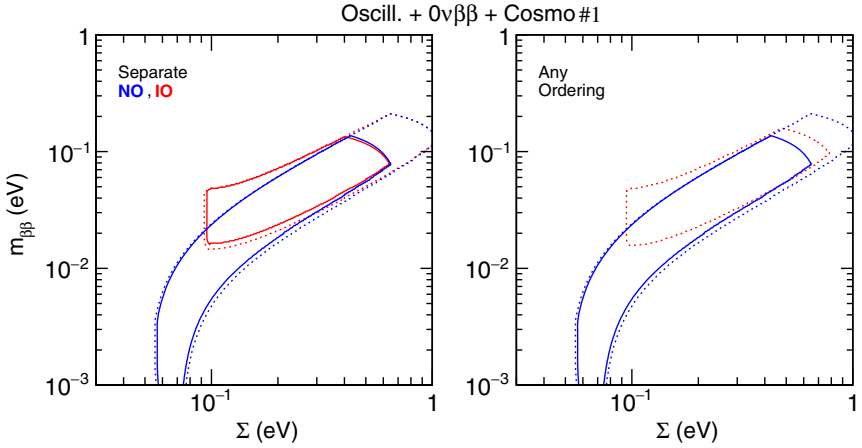

FIG. 7. As in Fig. 4, but including the $\chi^2(m_{\beta\beta})$ function from Fig. 2 and the $\chi^2(\Sigma)$ function from Fig. 3 (for case No. 1).

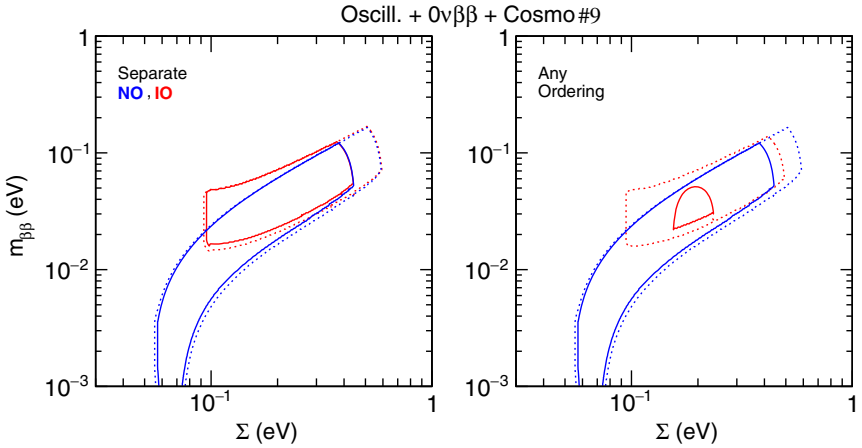

FIG. 8. As in Fig. 4, but including the $\chi^2(m_{\beta\beta})$ function from Fig. 2 and the $\chi^2(\Sigma)$ function from Fig. 3 (for case No. 9).

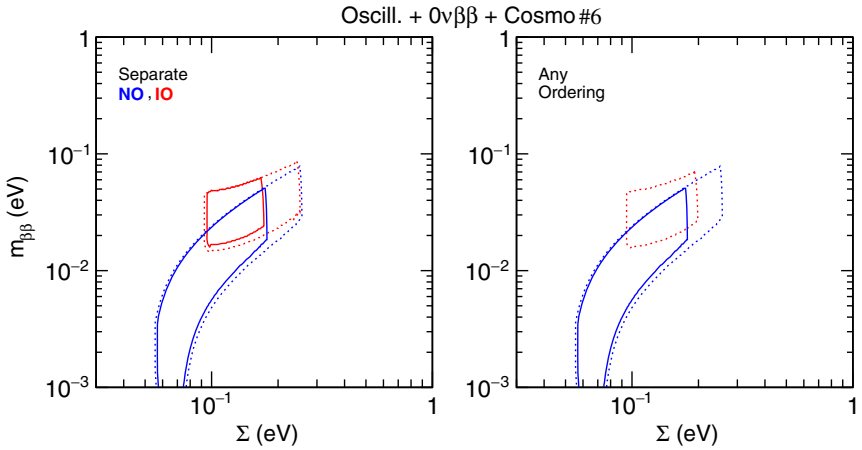

FIG. 9. As in Fig. 4, but including the $\chi^2(m_{\beta\beta})$ function from Fig. 2 and the $\chi^2(\Sigma)$ function from Fig. 3 (for case No. 6).

that the vertical width of the bands is mainly related to the unknown Majorana phases, while the oscillation parameter uncertainties play a secondary role that can be appreciated via the difference between the 2σ and 3σ allowed regions. By comparing the left and right panels in Fig. 4, one can notice that the NO regions are identical, while the IO region is slightly reduced on the right, due to the offset of the χ^2 minimum for IO in Eq. (9).

TABLE III. Values of $\Delta\chi^2_{\text{IO-NO}}$ from the global analysis of oscillation and nonoscillation data (numbered according to the adopted cosmological data sets as in Table II), to be compared with the value 3.6 from oscillation data only [Eq. (9)]. An overall preference emerges for NO, at the level of 1.9–2.1σ.

No.	1	2	3	4	5	6	7	8	9	10	11	12
$\Delta\chi^2_{\text{IO-NO}}$	4.3	3.8	4.4	4.2	3.9	4.4	3.6	3.7	3.8	3.7	3.8	3.9

Figure 5 is similar to Fig. 3, but includes the $0\nu\beta\beta$ constraints discussed in Sec. II B. In the left panel, both the NO and the IO allowed bands are horizontally cut at the $m_{\beta\beta}$ values in Eq. (13). In the right panel, the upper bounds on $m_{\beta\beta}$ are stronger in IO and can be estimated by drawing in Fig. 2 the lines at $\chi^2 = n^2 - 3.6$ ($n = 2, 3$), where 3.6 corresponds to the offset in Eq. (9). Note that, in the left panel, the projections of the NO and IO allowed regions onto the abscissa lead to upper bounds on Σ well above 1 eV.

Figure 6 includes, besides oscillation and $0\nu\beta\beta$ constraints, also the cosmological bounds for the case No. 10 in Sec. II C (see Table II). The left panel shows a synergic effect of $0\nu\beta\beta$ and cosmological data in setting a joint 2σ bound on Σ at the level of 0.9 eV, to be compared with the $0\nu\beta\beta$ bound (from Fig. 5) and the cosmological bound (from Table II, case No. 10), which are both above 1 eV. A more subtle synergy emerges from the fact that, for case No. 10, the $\chi^2(\Sigma)$ function is minimized at ~0.3 eV (see Fig. 3), well above the extrema in Eq. (14). Such a (relatively high) best-fit value for Σ implies preferred values $m_{\beta\beta}$ around few $\times 10^{-2}$ eV, as apparent for the IO region allowed at 2σ in the right panel. This relatively small IO 2σ region illustrates qualitatively how the constraints on $(\Sigma, m_{\beta\beta})$ would appear in the presence of a cosmological measurement (rather than of just upper bounds) for Σ.

Figures 7, 8, and 9 are analogous to Fig. 6, but refer to the cosmological data sets Nos. 1, 9, and 6 discussed in Sec. III C, respectively. Figure 7 shows, once more, the synergy between comparable $0\nu\beta\beta$ and cosmological bounds on Σ; indeed, in the left panel, one reads $\Sigma < 0.65$ eV, to be compared with $\Sigma < 0.72$–0.8 eV from cosmological data only (see Table II). In the right panel, there is no IO region allowed at 2σ, since the sum of the $\Delta\chi^2_{\text{IO-NO}}$ contributions from oscillation and cosmological data is $3.6 + 0.7 > 4.0$.

Figure 8 shows, in the left panel, the transition to a dominance of cosmological constraints on Σ: the 2σ bounds $\Sigma < 0.45$–046 eV for case No. 9 in Table II keep $m_{\beta\beta}$

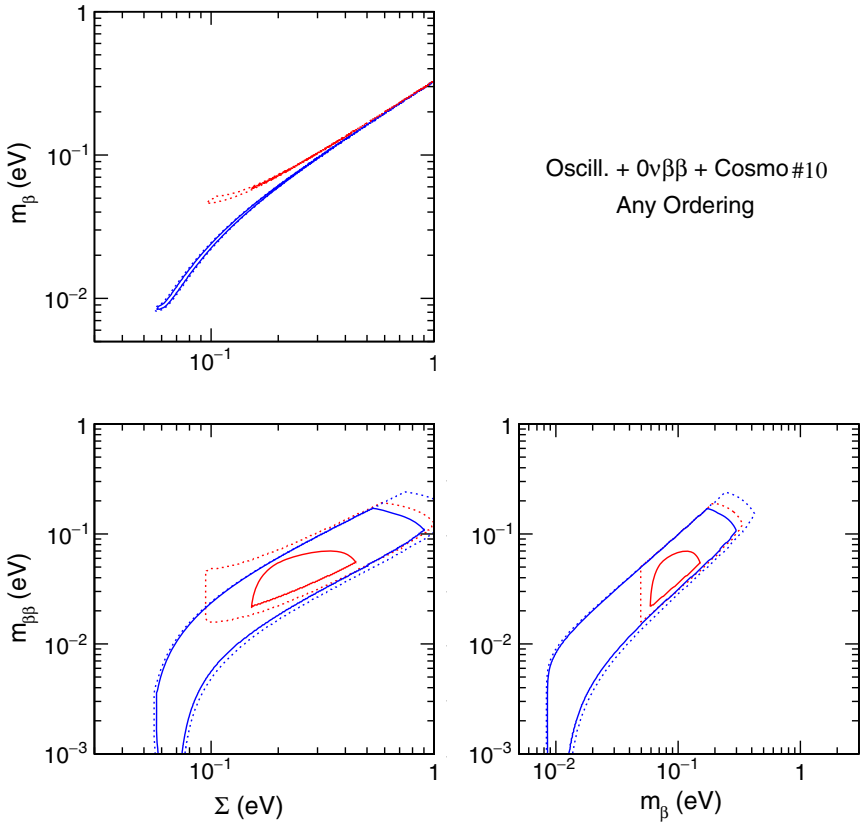

FIG. 10. Global 3ν analysis of neutrino oscillation and nonoscillation data, including the cosmological data set No. 10. Bounds in any mass ordering are shown at 2σ (solid curves) and 3σ (dotted curves), in the planes charted by any two among the three absolute mass observables $(\Sigma, m_{\beta\beta}, m_\beta)$.

sufficiently small to suppress any significant impact of current $0\nu\beta\beta$ data in the global fit. In the right panel, the relatively deep minimum of $\chi^2(\Sigma)$ evident in Fig. 3 leads to a 2σ allowed region in IO narrower than in Fig. 6. This region shows qualitatively the impact of prospective accurate measurement of Σ via cosmological data.

Figure 9 corresponds to the most constraining cosmological case (No. 6) in Table II. In this case, the allowed bands are almost vertically cut by the upper bounds on Σ from cosmological data only, with no significant contribution from $0\nu\beta\beta$ constraints. Indeed, the allowed values of $m_{\beta\beta}$ are well below the $0\nu\beta\beta$ bounds in Eq. (13). Note that, in the right panel, there is no region allowed at 2σ, since the global $\Delta\chi^2_{\text{IO-NO}}$ exceeds 4 units.

Table III reports the list of global $\Delta\chi^2_{\text{IO-NO}}$ values, numbered according to the cosmological cases in Table II. These values are not always equal to the algebraic sum of the $\Delta\chi^2$ contributions from oscillation data in Eq. (9) and cosmological data in Table II, since the best-fit points in the plane $(\Sigma, m_{\beta\beta})$ may be slightly readjusted in NO and IO in the global combination, leading to a small extra variation ($\delta\chi^2 \lesssim 0.4$). This minor effect in the combination of $0\nu\beta\beta$ and cosmological data is statistically insignificant at present, but might become more relevant with future data. In any case, Table III confirms that an overall preference for NO over IO emerges from the combination of oscillation and nonoscillation data, at the level of 1.9–2.1σ. This is one of the main results of our work.

We conclude this section with a remark on $m_{\beta\beta}$. In the above figures, the 2σ upper bounds on $m_{\beta\beta}$ decrease from <0.18 eV in Fig. 6 (dominated by KamLAND-Zen) to <0.06 eV in Fig. 9 (dominated by cosmology). There are good prospects to further probe this region—and possibly go below it—with upcoming or planned $0\nu\beta\beta$ experiments [53–55]. However, unlike Σ, there is no finite lower bound on $m_{\beta\beta}$, since the null value cannot be excluded *a priori* for unfavorable Majorana phases (see [102] and references therein). Conversely, a signal of $m_{\beta\beta} > 0$, if accurate enough, might provide some hints or even constraints on such phases (see, e.g., [103]). The identification of Majorana phases as a new source of leptonic *CP* violation (besides the Dirac phase δ) would open new perspectives on the role of leptons in the early universe (see [104] and references therein).

IV. IMPLICATIONS FOR m_β

The results obtained in the previous section have implications for the discovery potential of β-decay searches, such as the experiment KATRIN [105–107], designed to probe the range $m_\beta \gtrsim 0.2$ eV, or future projects, envisaged to reach potential sensitivities at or below 0.1 eV [20,108,109]. For the sake of brevity, we

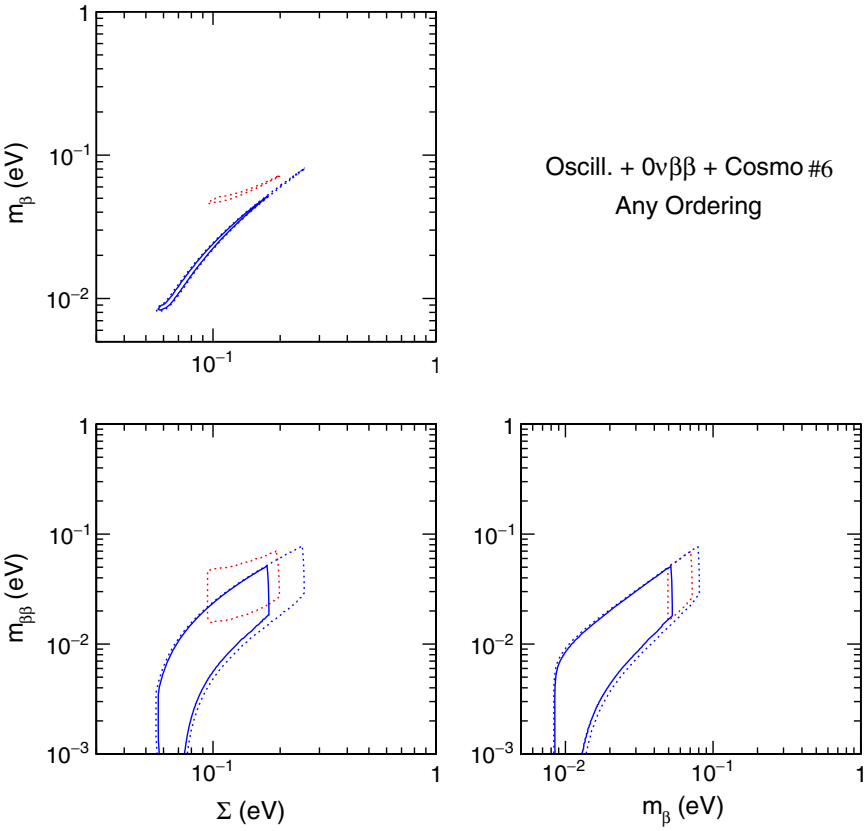

FIG. 11. As in Fig. 10, but including the cosmological data set No. 6.

consider only the case of global fit in any ordering and for two representative cosmological data sets, namely, Nos. 10 and 6 in Table II, that lead to conservative and aggressive bounds on Σ, respectively.

Figure 10 shows the bounds on any two among the three absolute mass observables $(\Sigma, m_{\beta\beta}, m_\beta)$ for case No. 10. The $(\Sigma, m_{\beta\beta})$ plane is identical to the right panel of Fig. 6, while the other two planes contain also the projected bounds on m_β. The allowed values of m_β extend up to $\sim$0.3 eV (2σ) and $\sim$0.4 eV (3σ), in the range testable by KATRIN; however, a large fraction of the m_β allowed range, including the preferred IO region at 2σ, is below the 0.2 eV sensitivity goal of this experiment.

Figure 11 is analogous to Fig. 10, but refers to the cosmological data set No. 6. In this case, the upper bound on Σ is very strong, and so is the bound on m_β. Indeed, in the (Σ, m_β) plane, the two allowed branches for NO and IO are completely disconnected and could, in principle, be conclusively discriminated via precise measurements of Σ and m_β. Unfortunately, the values of m_β required by such test are entirely below the KATRIN sensitivity [105], but, in the long term, they could be partly probed by planned or envisaged experimental projects [20,108,109].

V. CONCLUSIONS

We have performed a global analysis of oscillation and nonoscillation data within the standard three-neutrino framework. with particular attention to absolute neutrino masses and their ordering (either NO or IO). Oscillation data have been updated with the latest results, as available at the beginning of 2017. The $0\nu\beta\beta$ decay bounds have been derived by using recent results from the KamLAND-Zen experiment, together with a conservative evaluation of nuclear matrix elements and their uncertainties. Cosmological data from Planck and other experiments have been examined within the standard ΛCDM model, with allowance for nonzero neutrino masses (and eventually for an extra parameter). The cosmological analysis has been performed in a variety of cases, always considering the physical neutrino mass spectra for NO and IO.

In the global analysis, NO appears to be somewhat favored with respect to IO at the level of 1.9–2.1σ, mainly by neutrino oscillation data (especially atmospheric), corroborated by cosmological data in some cases. This intriguing indication, although not statistically mature yet, deserves to be monitored with future data. Detailed constraints on the neutrino mass-mixing parameter have also been obtained via the χ^2 method, by expanding the parameter space either around separate minima in NO and IO or around the absolute minimum in any ordering. Relevant results have been numerically summarized in Tables I–III and graphically shown in several figures. Implications for upcoming oscillation and nonoscillation neutrino experiments, including β-decay searches, have been discussed.

We emphasize that the above results have been obtained in the standard 3ν framework of massive and mixed neutrinos. The experimental search of oscillation phenomena, as well as of signals in the $(m_\beta, m_{\beta\beta}, \Sigma)$ parameter space should, however, be pursued independently of any 3ν expectations, which can be altered by new (sterile) neutrino states or by new (nonstandard) neutrino interactions, not considered in this work.

ACKNOWLEDGMENTS

This work is supported by the Italian Istituto Nazionale di Fisica Nucleare (INFN) and Ministero dell'Istruzione, Università e Ricerca (MIUR) through the "Theoretical Astroparticle Physics" projects. This work has also been performed within the Labex ILP (reference ANR-10-LABX-63) part of the Idex SUPER, and received financial state aid managed by the Agence Nationale de la Recherche, as part of the programme Investissements d'Avenir under the reference ANR-11-IDEX-0004-02. A. P. is supported by the project *Beyond three neutrino families* within the FutureInResearch program, Fondo di Sviluppo e Coesione 2007-2013, APQ Ricerca Regione Puglia "Programma regionale a sostegno della specializzazione intelligente e della sostenibilità sociale ed ambientale." F. C. is supported by NSF Grant No. PHY-1404311 to J. F. Beacom. E. L. thanks K. Inoue and Y. Koshio for communications about the recent KamLAND-Zen and Super-Kamiokande results, respectively.

[1] C. Patrignani *et al.* (Particle Data Group), Review of particle physics, Chin. Phys. C **40**, 100001 (2016); See the review by K. Nakamura and S. T. Petcov on Neutrino Mass, Mixing, and Oscillations therein.

[2] G. L. Fogli, E. Lisi, A. Marrone, and A. Palazzo, Global analysis of three-flavor neutrino masses and mixings, Prog. Part. Nucl. Phys. **57**, 742 (2006).

[3] R. B. Patterson, Prospects for measurement of the neutrino mass hierarchy, Annu. Rev. Nucl. Part. Sci. **65**, 177 (2015).

[4] X. Qian and P. Vogel, Neutrino mass hierarchy, Prog. Part. Nucl. Phys. **83**, 1 (2015).

[5] R. N. Mohapatra and A. Y. Smirnov, Neutrino mass and new physics, Annu. Rev. Nucl. Part. Sci. **56**, 569 (2006).

[6] F. Feruglio, Pieces of the flavour puzzle, Eur. Phys. J. C **75**, 373 (2015).
[7] S. F. King, Models of neutrino mass, mixing and *CP* violation, J. Phys. G **42**, 123001 (2015).
[8] G. L. Fogli and E. Lisi, Tests of three flavor mixing in long baseline neutrino oscillation experiments, Phys. Rev. D **54**, 3667 (1996).
[9] F. Capozzi, E. Lisi, A. Marrone, D. Montanino, and A. Palazzo, Neutrino masses and mixings: Status of known and unknown 3ν parameters, Nucl. Phys. **B908**, 218 (2016).
[10] F. Capozzi, E. Lisi, A. Marrone, D. Montanino, and A. Palazzo, Status and prospects of global analyses of neutrino mass-mixing parameters, in Neutrino 2016, XXVII International Conference on Neutrino Physics and Astrophysics, London, UK, 2016 [*J. Phys. Conf. Ser.* (to be published)], neutrino2016.iopconfs.org.
[11] I. Esteban, M. C. Gonzalez-Garcia, M. Maltoni, I. Martinez-Soler, and T. Schwetz, Updated fit to three neutrino mixing: Exploring the accelerator-reactor complementarity, J. High Energy Phys. 01 (2017) 087.
[12] D. V. Forero, M. Tortola, and J. W. F. Valle, Neutrino oscillations refitted, Phys. Rev. D **90**, 093006 (2014).
[13] S. M. Bilenky, C. Giunti, J. A. Grifols, and E. Masso, Absolute values of neutrino masses: Status and prospects, Phys. Rep. **379**, 69 (2003).
[14] E. W. Otten and C. Weinheimer, Neutrino mass limit from tritium beta decay, Rep. Prog. Phys. **71**, 086201 (2008).
[15] S. Dell'Oro, S. Marcocci, M. Viel, and F. Vissani, Neutrinoless double beta decay: 2015 review, Adv. High Energy Phys. **2016**, 2162659 (2016).
[16] S. Hannestad, Neutrino physics from precision cosmology, Prog. Part. Nucl. Phys. **65**, 185 (2010).
[17] A. Gando *et al.* (KamLAND-Zen Collaboration), Search for Majorana Neutrinos Near the Inverted Mass Hierarchy Region with KamLAND-Zen, Phys. Rev. Lett. **117**, 082503 (2016); Erratum, Phys. Rev. Lett. **117**,109903(E) (2016).
[18] J. Lesgourgues and S. Pastor, Neutrino cosmology and Planck, New J. Phys. **16**, 065002 (2014).
[19] P. A. R. Ade *et al.* (Planck Collaboration), Planck 2015 results. XIII. Cosmological parameters, Astron. Astrophys. **594**, A13 (2016).
[20] G. J. Barker *et al.*, The future of neutrino mass measurements: Terrestrial, astrophysical, and cosmological measurements in the next decade, arXiv:1309.7810.
[21] G. L. Fogli, E. Lisi, A. Marrone, A. Melchiorri, A. Palazzo, P. Serra, and J. Silk, Observables sensitive to absolute neutrino masses: Constraints and correlations from world neutrino data, Phys. Rev. D **70**, 113003 (2004).
[22] G. L. Fogli, E. Lisi, A. Marrone, A. Melchiorri, A. Palazzo, P. Serra, J. Silk, and A. Slosar, Observables sensitive to absolute neutrino masses: A reappraisal after WMAP-3y and first MINOS results, Phys. Rev. D **75**, 053001 (2007).
[23] G. L. Fogli, E. Lisi, A. Marrone, A. Melchiorri, A. Palazzo, A. M. Rotunno, P. Serra, J. Silk, and A. Slosar, Observables sensitive to absolute neutrino masses. II, Phys. Rev. D **78**, 033010 (2008).
[24] G. Cowan, Review on Statistics (Ref. [1]). See also F. James and M. Roos, Minuit: A system for function minimization and analysis of the parameter errors and correlations, Comput. Phys. Commun. **10**, 343 (1975).
[25] M. Blennow, P. Coloma, P. Huber, and T. Schwetz, Quantifying the sensitivity of oscillation experiments to the neutrino mass ordering, J. High Energy Phys. 03 (2014) 028.
[26] J. N. Bahcall, P. I. Krastev, and A. Y. Smirnov, Where do we stand with solar neutrino oscillations?, Phys. Rev. D **58**, 096016 (1998).
[27] S. T. Petcov, The solar neutrino problem and solar neutrino oscillations in vacuum and in matter, Lect. Notes Phys. **512**, 281 (1998).
[28] G. L. Fogli, E. Lisi, and D. Montanino, Matter enhanced three flavor oscillations and the solar neutrino problem, Phys. Rev. D **54**, 2048 (1996).
[29] A. de Gouvea, A. Friedland, and H. Murayama, The dark side of the solar neutrino parameter space, Phys. Lett. B **490**, 125 (2000).
[30] A. Friedland, MSW effects in vacuum oscillations, Phys. Rev. Lett. **85**, 936 (2000).
[31] E. Lisi, A. Marrone, D. Montanino, A. Palazzo, and S. T. Petcov, Analytical description of quasivacuum oscillations of solar neutrinos, Phys. Rev. D **63**, 093002 (2001).
[32] M. C. Gonzalez-Garcia, M. Maltoni, C. Pena-Garay, and J. W. F. Valle, Global three neutrino oscillation analysis of neutrino data, Phys. Rev. D **63**, 033005 (2001).
[33] G. L. Fogli, E. Lisi, A. Marrone, D. Montanino, and A. Palazzo, Getting the most from the statistical analysis of solar neutrino oscillations, Phys. Rev. D **66**, 053010 (2002).
[34] J. N. Bahcall, Solving the mystery of the missing neutrinos, arXiv:physics/0406040. Also available at www.nobelprize.org/nobel_prizes/themes/physics/bahcall.
[35] L. Lyons, Selecting between two hypotheses, Oxford University, Report No. OUNP-99-12, 1999; Statistical techniques in high energy physics, AIP Conf. Proc. **583**, 31 (2001).
[36] S. M. Bilenky, F. Capozzi, and S. T. Petcov, An alternative method of determining the neutrino mass ordering in reactor neutrino experiments, arXiv:1701.06328.
[37] F. Capozzi, E. Lisi, and A. Marrone, Neutrino mass hierarchy and electron neutrino oscillation parameters with one hundred thousand reactor events, Phys. Rev. D **89**, 013001 (2014).
[38] E. Ciuffoli, J. Evslin, and X. Zhang, Confidence in a neutrino mass hierarchy determination, J. High Energy Phys. 01 (2014) 095.
[39] M. Blennow, On the Bayesian approach to neutrino mass ordering, J. High Energy Phys. 01 (2014) 139.
[40] L. Stanco, S. Dusini, and M. Tenti, Determination of the neutrino mass hierarchy with a new statistical method, Phys. Rev. D **95**, 053002 (2017).
[41] M. C. Gonzalez-Garcia, M. Maltoni, and T. Schwetz, Updated fit to three neutrino mixing: Status of leptonic *CP* violation, J. High Energy Phys. 11 (2014) 052.
[42] K. Abe *et al.* (T2K Collaboration), First Combined Analysis of Neutrino and Antineutrino Oscillations at T2K, Phys. Rev. Lett. **118**, 151801 (2017).
[43] P. Adamson *et al.* (NOvA Collaboration), Constraints on oscillation parameters from ν_e appearance and ν_μ disappearance in NOvA, arXiv:1703.03328. See also P. Vahle, in Neutrino 2016 (Ref. [10]).

[44] P. Adamson *et al.* (NOvA Collaboration), Measurement of the Neutrino Mixing Angle θ_{23} in NOvA, Phys. Rev. Lett. **118**, 151802 (2017).

[45] F. P. An *et al.* (Daya Bay Collaboration), Improved measurement of the reactor antineutrino flux and spectrum at Daya Bay, Chin. Phys. C **41**, 013002 (2017); Measurement of electron antineutrino oscillation based on 1230 days of operation of the Daya Bay experiment, Phys. Rev. D **95**, 072006 (2017).

[46] Z. Li, Atmospheric neutrino results from Super-Kamiokande, *Proc. Sci.* ICHEP2016 (2016) 061.

[47] Y. Koshio, Solar and atmospheric neutrino oscillations in Super-Kamiokande, *Proc. Sci.* NOW2016 (2016) 001; https://pos.sissa.it/cgi-bin/reader/conf.cgi?confid=283.

[48] G. L. Fogli, E. Lisi, A. Marrone, A. Palazzo, and A. M. Rotunno, Hints of $\theta_{13} > 0$ from Global Neutrino Data Analysis, Phys. Rev. Lett. **101**, 141801 (2008).

[49] E. D. Kearns, 3-flavor oscillations with current and future atmospheric experiments, contribution to the April 2017 Meeting of the American Physical Society, Washington, DC, 2017, meetings.aps.org/Meeting/APR17/Session/J10.3.

[50] S. M. Bilenky and C. Giunti, Neutrinoless double-beta decay: A probe of physics beyond the standard model, Int. J. Mod. Phys. A **30**, 1530001 (2015).

[51] H. Päs and W. Rodejohann, Neutrinoless double beta decay, New J. Phys. **17**, 115010 (2015).

[52] J. D. Vergados, H. Ejiri, and F. Simkovic, Neutrinoless double beta decay and neutrino mass, Int. J. Mod. Phys. E **25**, 1630007 (2016).

[53] B. Schwingenheuer, Status and prospects of searches for neutrinoless double beta decay, Ann. Phys. (Berlin) **525**, 269 (2013).

[54] O. Cremonesi and M. Pavan, Challenges in double beta decay, Adv. High Energy Phys. **2014**, 951432 (2014).

[55] A. S. Barabash, Brief review of double beta decay experiments, arXiv:1702.06340.

[56] P. Vogel, Nuclear structure and double beta decay, J. Phys. G **39**, 124002 (2012).

[57] J. Hyvrinen and J. Suhonen, Nuclear matrix elements for $0\nu\beta\beta$ decays with light or heavy Majorana-neutrino exchange, Phys. Rev. C **91**, 024613 (2015).

[58] J. Engel and J. Menendez, Status and future of nuclear matrix elements for neutrinoless double-beta decay: A review, Rep. Prog. Phys. **80**, 046301 (2017).

[59] J. Ouellet, Results and status from KamLAND-Zen, *Proc. Sci.* ICHEP2016 (2016) 492; See also the talk online at indico.cern.ch/event/432527.

[60] E. Lisi, A. Rotunno, and F. Simkovic, Degeneracies of particle and nuclear physics uncertainties in neutrinoless $\beta\beta$ decay, Phys. Rev. D **92**, 093004 (2015).

[61] J. Barea, J. Kotila, and F. Iachello, Nuclear matrix elements for double-β decay, Phys. Rev. C **87**, 014315 (2013); $0\nu\beta\beta$ and $2\nu\beta\beta$ nuclear matrix elements in the interacting boson model with isospin restoration, Phys. Rev. C **91**, 034304 (2015).

[62] A. Faessler, G. L. Fogli, E. Lisi, V. Rodin, A. M. Rotunno, and F. Simkovic, QRPA uncertainties and their correlations in the analysis of $0\nu\beta\beta$ decay, Phys. Rev. D **79**, 053001 (2009).

[63] W. Hu, D. J. Eisenstein, and M. Tegmark, Weighing Neutrinos with Galaxy Surveys, Phys. Rev. Lett. **80**, 5255 (1998).

[64] A. D. Dolgov, Neutrinos in cosmology, Phys. Rep. **370**, 333 (2002).

[65] J. Lesgourgues and S. Pastor, Massive neutrinos and cosmology, Phys. Rep. **429**, 307 (2006).

[66] K. N. Abazajian *et al.*, Cosmological and astrophysical neutrino mass measurements, Astropart. Phys. **35**, 177 (2011).

[67] J. Lesgourgues and S. Pastor, Neutrino mass from cosmology, Adv. High Energy Phys. **2012**, 608515 (2012).

[68] S. Vagnozzi, E. Giusarma, O. Mena, K. Freese, M. Gerbino, S. Ho, and M. Lattanzi, Unveiling ν secrets with cosmological data: Neutrino masses and mass hierarchy, arXiv:1701.08172.

[69] E. Giusarma, M. Gerbino, O. Mena, S. Vagnozzi, S. Ho, and K. Freese, Improvement of cosmological neutrino mass bounds, Phys. Rev. D **94**, 083522 (2016).

[70] L. Xu and Q. G. Huang, Detecting the neutrinos mass hierarchy from cosmological data, arXiv:1611.05178.

[71] Q. G. Huang, K. Wang, and S. Wang, Constraints on the neutrino mass and mass hierarchy from cosmological observations, Eur. Phys. J. C **76**, 489 (2016).

[72] E. Di Valentino, E. Giusarma, O. Mena, A. Melchiorri, and J. Silk, Cosmological limits on neutrino unknowns versus low redshift priors, Phys. Rev. D **93**, 083527 (2016).

[73] A. J. Cuesta, V. Niro, and L. Verde, Neutrino mass limits: Robust information from the power spectrum of galaxy surveys, Phys. Dark Univ. **13**, 77 (2016).

[74] M. Archidiacono, T. Brinckmann, J. Lesgourgues, and V. Poulin, Physical effects involved in the measurements of neutrino masses with future cosmological data, J. Cosmol. Astropart. Phys. 02 (2017) 052.

[75] Y. Oyama, K. Kohri, and M. Hazumi, Constraints on the neutrino parameters by future cosmological 21 cm line and precise CMB polarization observations, J. Cosmol. Astropart. Phys. 02 (2016) 008.

[76] R. Allison, P. Caucal, E. Calabrese, J. Dunkley, and T. Louis, Towards a cosmological neutrino mass detection, Phys. Rev. D **92**, 123535 (2015).

[77] E. Di Valentino *et al.* (CORE Collaboration), Exploring cosmic origins with CORE: Cosmological parameters, arXiv:1612.00021.

[78] A. Banerjee, B. Jain, N. Dalal, and J. Shelton, Tests of neutrino and dark radiation models from galaxy and CMB surveys, arXiv:1612.07126.

[79] J. Hamann, S. Hannestad, and Y. Y. Y. Wong, Measuring neutrino masses with a future galaxy survey, J. Cosmol. Astropart. Phys. 11 (2012) 052.

[80] E. Di Valentino, A. Melchiorri, and J. Silk, Beyond six parameters: Extending ΛCDM, Phys. Rev. D **92**, 121302 (2015).

[81] E. Di Valentino, A. Melchiorri, and J. Silk, Reconciling Planck with the local value of H_0 in extended parameter space, Phys. Lett. B **761**, 242 (2016).

[82] H. Motohashi, A. A. Starobinsky, and J. Yokoyama, Cosmology Based on $f(R)$ Gravity Admits 1 eV Sterile Neutrinos, Phys. Rev. Lett. **110**, 121302 (2013).

[83] B. Hu, M. Raveri, A. Silvestri, and N. Frusciante, Exploring massive neutrinos in dark cosmologies with EFTCAMB/EFTCosmoMC, Phys. Rev. D **91**, 063524 (2015).
[84] S. Wang, Y. F. Wang, D. M. Xia, and X. Zhang, Impacts of dark energy on weighing neutrinos: Mass hierarchies considered, Phys. Rev. D **94**, 083519 (2016).
[85] X. Zhang, Impacts of dark energy on weighing neutrinos after Planck 2015, Phys. Rev. D **93**, 083011 (2016).
[86] N. Aghanim *et al.* (Planck Collaboration), Planck 2015 results. XI. CMB power spectra, likelihoods, and robustness of parameters, Astron. Astrophys. **594**, A11 (2016).
[87] N. Aghanim *et al.* (Planck Collaboration), Planck 2016 intermediate results. XLVI. Reduction of large-scale systematic effects in HFI polarization maps and estimation of the reionization optical depth, Astron. Astrophys. **596**, A107 (2016).
[88] F. Beutler, C. Blake, M. Colless, D. Heath Jones, L. Staveley-Smith, L. Campbell, Q. Parker, W. Saunders, and F. Watson, The 6dF Galaxy Survey: Baryon acoustic oscillations and the local Hubble constant, Mon. Not. R. Astron. Soc. **416**, 3017 (2011).
[89] A. J. Ross, L. Samushia, C. Howlett, W. J. Percival, A. Burden, and M. Manera, The clustering of the SDSS DR7 Main Galaxy Sample I: A 4 per cent distance measure at $z = 0.15$, Mon. Not. R. Astron. Soc. **449**, 835 (2015).
[90] L. Anderson *et al.* (BOSS Collaboration), The clustering of galaxies in the SDSS-III Baryon Oscillation Spectroscopic Survey: Baryon acoustic oscillations in the Data Releases 10 and 11 Galaxy samples, Mon. Not. R. Astron. Soc. **441**, 24 (2014).
[91] P. A. R. Ade *et al.* (Planck Collaboration), Planck 2015 results. XV. Gravitational lensing, Astron. Astrophys. **594**, A15 (2016).
[92] E. Calabrese, A. Slosar, A. Melchiorri, G. F. Smoot, and O. Zahn, Cosmic microwave weak lensing data as a test for the dark universe, Phys. Rev. D **77**, 123531 (2008).
[93] A. Lewis and S. Bridle, Cosmological parameters from CMB and other data: A Monte Carlo approach, Phys. Rev. D **66**, 103511 (2002); See http://cosmologist.info/cosmomc/
[94] A. Lewis, A. Challinor, and A. Lasenby, Efficient computation of CMB anisotropies in closed FRW models, Astrophys. J. **538**, 473 (2000).
[95] A. Lewis, Efficient sampling of fast and slow cosmological parameters, Phys. Rev. D **87**, 103529 (2013).
[96] J. Neyman, Outline of a theory of statistical estimation based on the classical theory of probability, Phil. Trans. R. Soc. A **236**, 333 (1937); reprinted in *A Selection of Early Statistical Papers on J. Neyman* (University of California Press, Berkeley, 1967).
[97] G. J. Feldman and R. D. Cousins, Unified approach to the classical statistical analysis of small signals, Phys. Rev. D **57**, 3873 (1998).
[98] W. Rodejohann, Neutrinoless double beta decay and neutrino physics, J. Phys. G **39**, 124008 (2012).
[99] S. Dell'Oro, S. Marcocci, and F. Vissani, New expectations and uncertainties on neutrinoless double beta decay, Phys. Rev. D **90**, 033005 (2014).
[100] S. Dell'Oro, S. Marcocci, M. Viel, and F. Vissani, The contribution of light Majorana neutrinos to neutrinoless double beta decay and cosmology, J. Cosmol. Astropart. Phys. 12 (2015) 023.
[101] C. Giunti and E. M. Zavanin, Predictions for neutrinoless double-beta decay in the $3 + 1$ sterile neutrino scenario, J. High Energy Phys. 07 (2015) 171.
[102] Z. z. Xing and Z. h. Zhao, The effective neutrino mass of neutrinoless double-beta decays: How possible to fall into a well, Eur. Phys. J. C **77**, 192 (2017).
[103] H. Minakata, H. Nunokawa, and A. A. Quiroga, Constraining Majorana *CP* phase in the precision era of cosmology and the double beta decay experiment, Prog. Theor. Exp. Phys. **2015**, 033B03 (2015).
[104] S. Pascoli, S. T. Petcov, and A. Riotto, Leptogenesis and low energy *CP* violation in neutrino physics, Nucl. Phys. **B774**, 1 (2007).
[105] J. Angrik *et al.* (KATRIN Collaboration), KATRIN Design Report, 2004 (245 p.); Reports No. FZKA-7090, No. NPI ASCR Rez EXP-01/2005, and No. MS-KP-0501; available at www.katrin.kit.edu.
[106] E. W. Otten and C. Weinheimer, Neutrino mass limit from tritium beta decay, Rep. Prog. Phys. **71**, 086201 (2008).
[107] G. Drexlin, in NOW 2016 (Ref. [47]), see http://www.ba.infn.it/now.
[108] L. Gastaldo, *Proc. Sci.* NOW2016 (2016) 060; https://pos.sissa.it/cgi-bin/reader/conf.cgi?confid=283.
[109] A. A. Esfahani *et al.*, Determining the neutrino mass with cyclotron radiation emission spectroscopy—Project 8, J. Phys. G **44**, 054004 (2017).